A versatile femtosecond stimulated Raman spectroscopy setup with tunable pulses in the visible to near infrared

Citation	Zhu, L., Liu, W., & Fang, C. (2014). A versatile femtosecond stimulated Raman spectroscopy setup with tunable pulses in the visible to near infrared. Applied Physics Letters, 105(4), 041106. doi:10.1063/1.4891766
DOI	10.1063/1.4891766
Publisher	American Institute of Physics Publishing
Version	Version of Record
Terms of Use	http://cdss.library.oregonstate.edu/sa-termsofuse

A versatile femtosecond stimulated Raman spectroscopy setup with tunable pulses in the visible to near infrared

Liangdong Zhu (朱良栋),[1] Weimin Liu (刘伟民),[2] and Chong Fang (方翀)[1,2,a)]
[1]Department of Physics, Oregon State University, Corvallis, Oregon 97331, USA
[2]Department of Chemistry, Oregon State University, Corvallis, Oregon 97331, USA

(Received 9 June 2014; accepted 20 July 2014; published online 28 July 2014)

We demonstrate a versatile and efficient setup to perform femtosecond stimulated Raman spectroscopy (FSRS). Technical innovations are implemented to achieve the wavelength tunability for both the picosecond narrowband Raman pump pulse and femtosecond broadband Raman probe pulse. Using a simplified one-grating scheme in a home-built second harmonic bandwidth compressor followed by a two-stage noncollinear optical parametric amplifier, we tune the Raman pump pulse from ca. 480 to 750 nm. To generate the suitable Raman probe pulse in tandem, we rely on our recently demonstrated broadband up-converted multicolor array technique that readily provides tunable broadband laser sidebands across the visible to near-infrared range. This unique setup has unparalleled flexibility for conducting FSRS. We measure the ground-state Raman spectra of a cyclohexane standard using tunable pump-probe pairs at various wavelengths across the visible region. The best spectral resolution is $\sim$12 cm^{-1}. By tuning the pump wavelength closer to the electronic absorption band of a photoacid pyranine in water, we observe the pre-resonantly enhanced Raman signal. The stimulated Raman gain of the 1627 cm^{-1} mode is increased by over 15 times.
 [http://dx.doi.org/10.1063/1.4891766]

Ultrafast spectroscopic techniques are powerful in tackling some of the most challenging problems in modern physics, chemistry, biology, and materials science with the advancement of femtosecond (fs) laser technologies.[1–4] Using sophisticated sequence of laser pulses in specific geometries, researchers can unravel the microscopic atomic motions that play a crucial role leading to macroscopic functions. The key is to capture molecular structural snapshots with simultaneously high spectral and temporal resolution. In particular, studies of photophysical and photochemical events in life processes including photosynthesis and fluorescence as well as photolysis of metal-organic complexes in materials science demand a technique that can access nuclear coordinates in the electronic excited state.

In contrast to the commonly used transient absorption that infers molecular speciation in the electronic domain,[5–7] femtosecond stimulated Raman spectroscopy (FSRS) is an emerging structural dynamics technique that can acquire high signal-to-noise ratio excited-state vibrational spectrum free from fluorescence background.[3,8–10] In FSRS, a picosecond (ps) narrowband Raman pump (R_{pu}) pulse and an fs broadband probe pulse are used to stimulate Raman scattering signals and produce sharp vibrational features across a wide spectral region. Since the resultant FSRS spectrum is obtained based on the equation, Raman gain = Raman probe spectrum with pump on/Raman probe spectrum with pump off − 1, a combination of 500-Hz optical chopper in the pump arm and a charge coupled device (CCD) camera synchronized with the 1-kHz laser repetition rate ensures that one stimulated Raman spectrum can be obtained in 2 ms.[11,12] Large quantities of data traces can thus be efficiently collected and averaged to improve the signal-to-noise ratio. Further advantages of using FSRS to study molecular motions either in the ground state or excited state are accomplished by tuning the Raman pump and probe pulses across a broad spectral range. One can make use of resonance enhancement with a tunable pump[13–18] to increase the Raman signal, in conjunction with the probe improvement of generating a tunable broadband pulse to access the low-frequency region[10,19] as compared to conventional continuous-wave Raman or IR spectroscopy.

In this Letter, we demonstrate an improved FSRS setup [Fig. 1] that can simultaneously tune the R_{pu} pulse in the visible (ca. 480–750 nm) and the accompanying Raman probe (R_{pr}) pulse in the visible to near IR (ca. 450–850 nm). Notably, the broad spectral coverage is continuous without gaps. Briefly, the fs laser system consists of a mode-locked Ti:Sapphire oscillator (Mantis-5) and regenerative amplifier (Legend Elite-USP-1 K-HE, Coherent) that provides $\sim$4 W fundamental pulse (FP) at 800 nm (35 fs, 1 kHz). About 1.6 mJ/pulse FP is used to generate the tunable pulses for FSRS. The R_{pu} generation consists of three parts: (1) second-harmonic bandwidth compressor (SHBC) that produces a 400-nm narrowband ps pump; (2) femtosecond noncollinear optical parametric amplifier (NOPA) and grating-slit-based spectral filter[13] that produce narrowband ps seed with wavelength tunability; and (3) a two-stage ps-NOPA that amplifies the ps seed with the ps pump to generate the intense, tunable ps R_{pu} output. In parallel, a broadband up-converted multicolor array (BUMA) setup provides a tunable broadband fs pulse as R_{pr}. Both the R_{pu} and R_{pr} pulses are then combined noncollinearly to perform ground-state FSRS measurements.[4,11,12]

The BUMA signal has been used as R_{pr} to collect an anti-Stokes Raman spectrum of a solvent mixture with R_{pu} = 800 nm.[10] Here, we aim to exploit the full potential of BUMA technology in tunable FSRS. In the BUMA setup

a)Author to whom correspondence should be addressed. Electronic mail: Chong.Fang@oregonstate.edu.

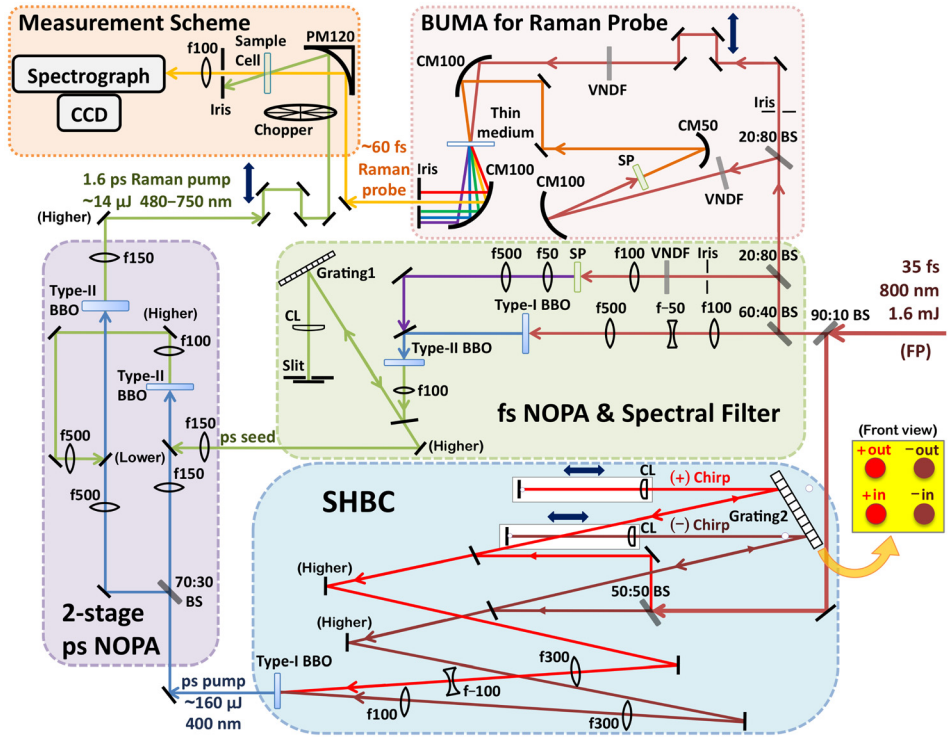

FIG. 1. Schematic (top-view) of our experimental setup to perform tunable FSRS. The 800 nm FP powers three distinct parts: SHBC (light blue shade), fs NOPA and spectral filter (light green), and BUMA apparatus (light red). The ps pump and seed pulses are combined in the two-stage single-pass ps NOPA (light violet) to generate tunable, ps Raman pump pulse in the visible. The Raman ps pump and fs probe pulses interrogate the sample in the measurement scheme (light orange). SP, sapphire plate; VNDF, variable neutral-density filter; BS, beamsplitter; f100, lens with focal length of 100 mm; CM, concave mirror; CL, cylindrical lens; PM, parabolic mirror. Grating1 (2) denotes the plane-ruled reflective grating with 1800 (1200) grooves/mm and 500 (1000) nm blaze. Most delay lines for time overlap are omitted for simplicity. The four-beam geometry on the single grating in SHBC is depicted on the right (yellow). The focal points are marked by small white circles beside Grating2. The 90:10 BS represents 90% Reflection, 10% Transmission. In the NOPA setup, the *p*-polarized visible seed and *s*-polarized 400-nm pump beams are vertically displaced and overlapped in type-II BBO in a noncollinear geometry with a crossing angle of ~3°.

[Fig. 1, light red area], ~75 μJ/pulse FP passes through a 20R:80T beamsplitter. The reflected arm is focused on a 2-mm-thick *Z*-cut single-crystal sapphire plate to generate supercontinuum white light (SCWL). The transmitted arm is attenuated before being focused on a 0.5-mm-thick transparent medium[19–23] (e.g., quartz plate) to noncollinearly pump SCWL with a crossing angle of ~6°. The diameters of both beams on the quartz surface are ~200 μm. We use quartz due to its high optical damage threshold.[24] Depending on the R_{pu} wavelength, one of the first three BUMA sidebands (S_{+1} for $R_{pu} > 600$ nm, S_{+2} for $520 \le R_{pu} \le 600$ nm, and S_{+3} for $R_{pu} < 520$ nm) is selected as R_{pr}. All the sidebands have the same *p*-polarization as the incident SCWL.

The advantages of the BUMA probe over the commonly used SCWL are the following. (1) Wavelength tunability is achieved by varying the time delay between the two incident pulses. (2) It is background free because the sidebands are spatially separated from FP. Traditionally, a broadband probe near 800 nm is difficult to obtain because of strong interference between the nascent SCWL and residual 800-nm FP. This limits our capabilities to investigate molecular systems with interesting electronic and/or vibrational features in this spectral regime. BUMA sidebands fill the void and the influence from residual FP can be minimized.[4] (3) BUMA sidebands are self-compressed to ca. 30–60 fs pulse duration[19,23] so no additional compression is needed, in contrast to the complex compression system required for SCWL.[9,11] (4) Parametric amplification based on $\chi^{(3)}$ and $\chi^{(2)}$-nonlinearities[25] increases the sideband signal intensity so higher signal-to-noise ratio in FSRS can be achieved. Furthermore, compared to the NOPA probe,[15] the BUMA probe offers subsequent benefits. (i) It is economical and flexible.[10,19,23,25–27] Depending on applications such as fs Raman or optical switching, various media can be used that include beta barium borate (BBO), sapphire, CaF_2, quartz, BK7 glass, etc. (ii) Broadband sidebands are readily achieved and potentially on either side of FP.[25] It does not require precise tuning of the phase-matching angle[28] or manipulation of the input beams.[21,29]

To generate the intense ps R_{pu} from an fs laser source, several conversion stages are needed. In the green shaded area of Fig. 1, ~20 μJ of FP is attenuated and focused onto a 2-mm-thick sapphire plate to generate SCWL. About 60 μJ of FP undergoes beam size reduction through a telescope and frequency doubling in a 1-mm-thick type-I BBO to generate ~20 μJ SH pulses. The SCWL and 400-nm pulses are focused onto a 1-mm-thick type-II BBO as the signal and pump, respectively, in an fs-NOPA setup. The center wavelength of the amplified signal is tunable from ca. 480 to 750 nm via rotating the BBO crystal and adjusting the time delay between the two incident pulses. The NOPA output (~1 μJ/pulse) is dispersed by a reflective grating (1800 grooves/mm, 500 nm blaze at 26.7°; 10RG1800–500-1, Newport) and focused on an adjustable slit by a cylindrical lens (CL) to select a portion with ~12 cm^{-1} bandwidth.[13,14] The spectrally filtered pulse is used in the subsequent two-stage ps-NOPA as the ps seed.

Based on the effect of chirp elimination in second-harmonic generation (SHG) when the incident FPs have opposite temporal chirps,[30,31] chirp-free 400-nm ps pump is generated in a homemade SHBC [Fig. 1, light blue area]. The input FP is evenly split into the positive and negative-chirp arms. Instead of using one grating per arm,[15–17] we achieve a compact and economical setup with just one reflective grating (1200 grooves/mm, 1000 nm blaze at 36.8°; 20RG1200–1000-2, Newport). In each arm, a CL and a back mirror on the focal point of the CL are placed on a translation stage. Dispersion depends on the distance between the CL and grating (denoted as d_1/d_2 for the positive/negative-chirp arm). The two translation stages are placed that d_1/d_2 is smaller/larger than the CL focal length. To generate a chirp-free SH pulse, d_1 and d_2 need to be tuned to equalize the magnitude of the two opposite chirps. Experimentally, this is achieved by sending one FP into both arms consecutively, and the duration of the output matches input when the two opposite chirps cancel each other.[32] The two chirped pulses are then telescoped to smaller beam sizes (~2 mm diameter)[15] and combined noncollinearly on a 1-mm-thick type-I BBO to generate the 400 nm, ~160 μJ, 2 ps SH pulse. Considering that each incident chirped-FP energy is ~300 μJ, the conversion efficiency reaches ~27%.

The SHBC output is divided by a beamsplitter (70%R) to pump a two-stage ps-NOPA system [Fig. 1, light violet area] that ensures high conversion efficiency and output stability. The ps seed is amplified in the first ps-NOPA (3-mm-thick type-II BBO) to ~1 μJ, and further amplified up to 14 μJ in the second ps-NOPA (5-mm-thick type-II BBO). This represents an overall conversion efficiency of ~1% (from fs FP to ps R_{pu}) that is adequate.[13–15,17] Higher efficiency can be obtained by changing the SHBC grating blaze [Fig. 1] from 1 μm to 800 nm. After collimation, the ps pulse is ready to be used as the narrowband R_{pu} for tunable FSRS.

To characterize the ps R_{pu}, we measure its spectrum (e.g., centered at ~599 nm) using an Ocean Optics spectrometer (QE65-Pro, spectral range 520–690 nm) [Fig. 2(a)]. The full-width-at-half-maximum (FWHM) is 1.02 nm (27.8 cm^{-1}). The pulse duration is obtained by a home-built SHG-autocorrelator with a 0.1-mm-thick type-I BBO. The FWHM of the autocorrelation signal is 2.27 ps [Fig. 2(b)], corresponding to an incident pulse duration of ~1.6 ps. Autocorrelation profiles for other R_{pu} wavelengths [Fig. 3(a)] are similar. The near-Gaussian temporal profile improves spectral resolution while minimizing unwanted spectral ringing in FSRS data.[18] The time-bandwidth product of ~44.5 ps·cm^{-1} is ~3 times the Fourier-transform limit of a Gaussian pulse (14.7 ps·cm^{-1}),[14,17] indicative of a chirped R_{pu}. However, by adjusting the temporal and spatial overlap between the collimated Raman pump-probe pair, we can obtain high-quality FSRS data without the need to achieve the narrowest bandwidth for a chirp-free R_{pu}. This is because the broadband fs-R_{pr} induces the vibrational coherence only with a specific portion of R_{pu} during their time overlap,[9,11] and the amount of R_{pu} temporal chirp occurring during the vibrational dephasing time is significantly less than the vibrational linewidth.[3,33] Therefore, the distorted FSRS lineshape is not apparent (see below).

In the measurement scheme [Fig. 1, light orange area], the *p*-polarized R_{pu} and R_{pr} are spatially and temporally overlapped at the sample cell in a crossing geometry. The transmitted R_{pr} carrying the stimulated Raman scattering signal is dispersed by a 600-grooves/mm grating (400 nm blaze) in a spectrograph (MS127i, Oriel) and focused onto a CCD-array camera (PIXIS 100F, Princeton Instruments) synchronized at the laser repetition rate. Instrument control and initial data processing are performed by LabVIEW.

To examine the tunability of our setup, we collect the ground-state FSRS spectra of cyclohexane (a solvent standard) at six different R_{pu} wavelengths with the power of 12 ± 1 μJ/pulse. The broad tunable range of R_{pu}-R_{pr} pairs is exhibited in Fig. 3, and resultant Raman spectra are shown in Fig. 4. The FWHM of the 802 cm^{-1} mode varies from 27 cm^{-1} (R_{pu} = 483 nm) to 12 cm^{-1} (R_{pu} = 745 nm). The main factor that increases the R_{pu} bandwidth is spectral broadening by the ps-NOPA processes. In particular, the precision limit of the grating-mechanical-slit filter yields a broader R_{pu} bandwidth at shorter wavelengths. The small ringing near the main peak is likely due to our ~1.6 ps R_{pu} that still truncates the mode free induction decay (dephasing time of ~2.0 ps). Additional spectral filtering of R_{pu} has shown to be useful.[18] The 802 cm^{-1} mode gain varies from 28% (R_{pu} = 652 nm) to 44% (R_{pu} = 483 nm), displaying no clear trend versus the R_{pu}

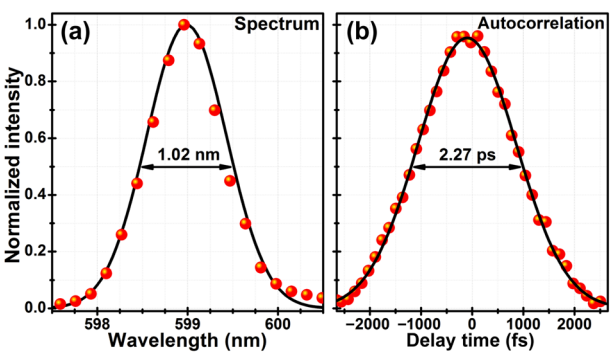

FIG. 2. Characterization of a typical narrowband R_{pu} pulse. The spectral (a) and temporal (b) profile of the R_{pu} centered at 599 nm. Red spheres represent experimental data while black solid lines are Gaussian fits. The FWHM values are indicated.

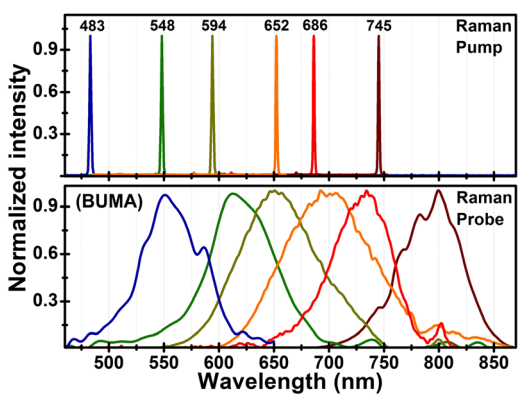

FIG. 3. Broad tunability of the R_{pu} and R_{pr} pulses in pairs. Normalized experimental R_{pu} spectra at six different center wavelengths: 483, 548, 594, 652, 686, and 745 nm (top) and the corresponding R_{pr} spectra from BUMA sidebands (bottom). By tuning the BUMA apparatus and choosing the order of sidebands to cover various spectral regions, we can conveniently collect the stimulated Raman spectrum spanning from ca. 100–4000 cm^{-1} at each R_{pu} wavelength.

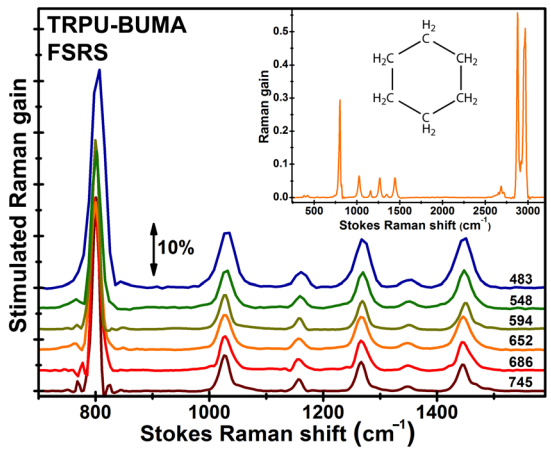

FIG. 4. Ground-state FSRS spectra of cyclohexane collected at six different R_{pu} wavelengths. TRPU: tunable Raman pump. The inset shows the FSRS spectrum ($R_{pu} = 652$ nm) spanning an ultrabroad range (ca. 200–3500 cm^{-1}). The chemical structure of cyclohexane is depicted. The double-sided arrow represents the Raman gain magnitude of 10%.

wavelength. Meanwhile, the intensity ratios between the 802, 1028, 1266, and 1445 cm^{-1} peaks remain unchanged throughout wavelength tuning, consistent with the intensity-corrected standard cyclohexane Raman spectrum acquired using 532 and 752-nm excitation.[34]

One major motivation to develop tunable FSRS is to exploit resonance enhancement to increase the signal-to-noise ratio of Raman spectrum.[35–37] We measure the ground-state FSRS signal of 10-mM photoacid pyranine (8-hydroxypyrene-1,3,6-trisulfonic acid, or HPTS)[11,12,38] in water [Fig. 5]. Seven different R_{pu} wavelengths are used and the corresponding 1627 cm^{-1} mode intensities are plotted in Fig. 5 inset. The vibrational modes of HPTS are clearly resolved with different intensity ratios from previous results[12] at $R_{pu} = 800$ nm. The intensity ratio of the 1627 over 1368 cm^{-1} modes drops from 2:1 at 483-nm pump to 3:2 at 745-nm pump. These findings are indicative of mode-dependent Raman excitation profiles that lead to relative Raman intensity changes as a function of excitation wavelength.[37] To minimize influence from the

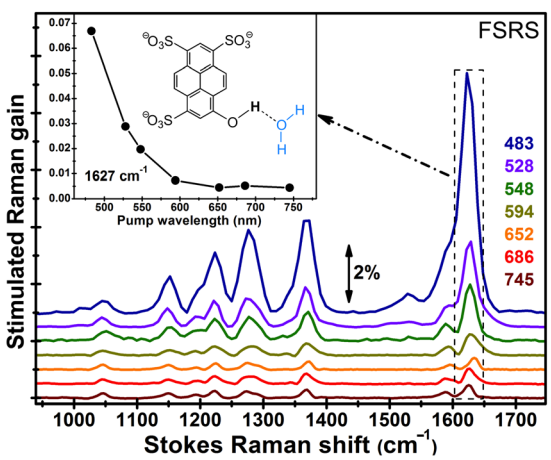

FIG. 5. Ground-state FSRS spectra of pyranine (HPTS) collected at seven different R_{pu} wavelengths of 483, 528, 548, 594, 652, 686, and 745 nm. The amplitude of the strongest Raman peak at 1627 cm^{-1} is plotted against R_{pu} wavelength in the inset, where the chemical structure of HPTS molecule in H-bonding configuration with a nearby water molecule is illustrated. The double-sided arrow represents the Raman gain magnitude of 2%.

overlapping lower-frequency shoulder, we use multi-Gaussian fitting to retrieve the peak height of the main band. The Raman gain of 0.44% at $R_{pu} = 745$ nm is similar to the aforementioned $R_{pu} = 800$ nm data (0.22%). When R_{pu} is blue-tuned to 594 nm, small enhancement is observed (0.73% gain). As R_{pu} is tuned toward the ~400-nm electronic absorption band of HPTS in water,[12,38] strong pre-resonance enhancement occurs: the 1627 cm^{-1} mode gain is ~2.0%, 2.9%, and 6.7% for $R_{pu} = 548$, 528, and 483 nm, respectively. Therefore, >15 times increase of the Raman gain is observed upon tuning R_{pu} from 745 to 483 nm. Signal enhancement is especially useful when the intrinsic Raman cross-section is small, and with an additional actinic pump to photoexcite the sample, we can better capture spectral signatures of transient species during chemical reactions such as excited-state proton transfer in biomolecules.[3,39]

In summary, we present a unique FSRS setup with simultaneously tunable Raman pump and probe pulses in the visible from a single fs source. The narrowband ps Raman pump (480–750 nm, up to 14 μJ/pulse) offers the highest power among reported tunable FSRS setups,[13–18] while the SHBC design with one grating gives improved simplicity. The broadband fs Raman probe (450–850 nm, <100 nJ/pulse) arises from the spatially separated BUMA sidebands, which provide ultrabroad tunability with self-compression rooted in cascaded four-wave mixing.[20,23] In principle, we can extend the probe into the ultraviolet regime (i.e., <400 nm) using sum-frequency-generation/SHG-induced BUMA signals.[23,27,32] The convenience and versatility to broadly tune R_{pu}-R_{pr} pairs are manifested through the measurement of ground-state Raman spectrum of cyclohexane. Moreover, we achieve the pre-resonance enhancement of pyranine FSRS signals in aqueous solution by tuning R_{pu} toward the electronic absorption peak and the R_{pr} spectral profile in tandem. The combination of tunable ps and fs pulses from a commercially available fs-laser source will enable the elucidation of ultrafast structural dynamics by monitoring transient species with desirable specificity and sensitivity on the atomic level, thus paving the way for FSRS to be widely employed to tackle challenging problems[2–4,39] in materials, energy, and life sciences.

This work was funded by the Oregon State University faculty research startup grant to C. Fang. We thank Dr. Oksana Ostroverkhova and Dr. Sean Burrows for additional instrument support.

[1]G. S. Engel, T. R. Calhoun, E. L. Read, T.-K. Ahn, T. Mancal, Y.-C. Cheng, R. E. Blankenship, and G. R. Fleming, Nature **446**, 782 (2007).
[2]R. M. Hochstrasser, Proc. Natl. Acad. Sci. U.S.A. **104**, 14190 (2007).
[3]C. Fang, R. R. Frontiera, R. Tran, and R. A. Mathies, Nature **462**, 200 (2009).
[4]W. Wang, W. Liu, I.-Y. Chang, L. A. Wills, L. N. Zakharov, S. W. Boettcher, P. H.-Y. Cheong, C. Fang, and D. A. Keszler, Proc. Natl. Acad. Sci. U.S.A. **110**, 18397 (2013).
[5]L. Zhu, J. T. Sage, and P. M. Champion, Science **266**, 629 (1994).
[6]M. Chattoraj, B. A. King, G. U. Bublitz, and S. G. Boxer, Proc. Natl. Acad. Sci. U.S.A. **93**, 8362 (1996).
[7]R. Berera, R. Grondelle, and J. M. Kennis, Photosynth. Res. **101**, 105 (2009).
[8]M. Yoshizawa and M. Kurosawa, Phys. Rev. A **61**, 013808 (1999).
[9]D. W. McCamant, P. Kukura, S. Yoon, and R. A. Mathies, Rev. Sci. Instrum. **75**, 4971 (2004).

[10]L. Zhu, W. Liu, and C. Fang, Appl. Phys. Lett. **103**, 061110 (2013).
[11]W. Liu, F. Han, C. Smith, and C. Fang, J. Phys. Chem. B **116**, 10535 (2012).
[12]F. Han, W. Liu, and C. Fang, Chem. Phys. **422**, 204 (2013).
[13]S. Shim and R. A. Mathies, Appl. Phys. Lett. **89**, 121124 (2006).
[14]D. T. Co, J. V. Lockard, D. W. McCamant, and M. R. Wasielewski, Appl. Opt. **49**, 1880 (2010).
[15]S. A. Kovalenko, A. L. Dobryakov, and N. P. Ernsting, Rev. Sci. Instrum. **82**, 063102 (2011).
[16]H. Kuramochi, S. Takeuchi, and T. Tahara, J. Phys. Chem. Lett. **3**, 2025 (2012).
[17]M. Nejbauer and C. Radzewicz, Opt. Express **20**, 2136 (2012).
[18]E. Pontecorvo, C. Ferrante, C. G. Elles, and T. Scopigno, Opt. Express **21**, 6866 (2013).
[19]W. Liu, L. Zhu, L. Wang, and C. Fang, Opt. Lett. **38**, 1772 (2013).
[20]H. Crespo, J. T. Mendonca, and A. Dos Santos, Opt. Lett. **25**, 829 (2000).
[21]J. Liu and T. Kobayashi, Opt. Express **16**, 22119 (2008).
[22]M. Zhi, X. Wang, and A. V. Sokolov, Opt. Express **16**, 12139 (2008).
[23]W. Liu, L. Zhu, and C. Fang, Opt. Lett. **37**, 3783 (2012).
[24]A. A. Said, T. Xia, A. Dogariu, D. J. Hagan, M. J. Soileau, E. W. Van Stryland, and M. Mohebi, Appl. Opt. **34**, 3374 (1995).
[25]L. Zhu, W. Liu, L. Wang, and C. Fang, Laser Phys. Lett. **11**, 075301 (2014).
[26]W. Liu, L. Wang, F. Han, and C. Fang, Opt. Lett. **38**, 3304 (2013).
[27]W. Liu, L. Wang, and C. Fang, Appl. Phys. Lett. **104**, 111114 (2014).
[28]G. Cerullo and S. D. Silvestri, Rev. Sci. Instrum. **74**, 1 (2003).
[29]D. V. Khakhulin, A. B. Savel'ev, and R. V. Volkov, Laser Phys. Lett. **4**, 345 (2007).
[30]O. E. Martinez, J. Opt. Soc. Am. B **3**, 929 (1986).
[31]F. Raoult, A. C. L. Boscheron, D. Husson, C. Sauteret, A. Modena, V. Malka, F. Dorchies, and A. Migus, Opt. Lett. **23**, 1117 (1998).
[32]S. Laimgruber, H. Schachenmayr, B. Schmidt, W. Zinth, and P. Gilch, Appl. Phys. B **85**, 557 (2006).
[33]P. Kukura, D. W. McCamant, S. Yoon, D. B. Wandschneider, and R. A. Mathies, Science **310**, 1006 (2005).
[34]I. R. Lewis and H. Edwards, *Handbook of Raman Spectroscopy: From the Research Laboratory to the Process Line*, 1st ed. (CRC Press, New York, NY, 2001).
[35]A. B. Myers and R. A. Mathies, in *Biological Applications of Raman Spectroscopy*, edited by T. G. Spiro (John Wiley & Sons, Inc., New York, 1987), Vol. 2, pp. 1.
[36]R. P. McLaughlin, B. P. Nyholm, and P. J. Reid, J. Phys. Chem. A **107**, 9105 (2003).
[37]S. Shim, C. M. Stuart, and R. A. Mathies, Chem. Phys. Chem. **9**, 697 (2008).
[38]Y. Wang, W. Liu, L. Tang, B. G. Oscar, F. Han, and C. Fang, J. Phys. Chem. A **117**, 6024 (2013).
[39]B. G. Oscar, W. Liu, Y. Zhao, L. Tang, Y. Wang, R. E. Campbell, and C. Fang, Proc. Natl. Acad. Sci. U.S.A. **111**, 10191 (2014).